STUDY OF HYDROGEN-DEFECT INTERACTION IN THIN Nb FILM ON Si SUBSTRATE USING POSITRON ANNIHILATION

J. Čížek[1], I. Procházka[1], G. Brauer[2], W. Anwand[2], A. Mücklich[2], R. Kirchheim[3], A. Pundt[3], C. Bäthz[4], M. Knapp[4]

[1] *Department of Low-Temperature Physics, Faculty of Mathematics and Physics, Charles University, CZ-18000 V Holešovičkách 2, Praha 8, Czech Republic*
[2] *Institut für Ionenstrahlphysik und Materialforschung, Forschungszentrum Rossendorf, Postfach 510119, D-01314 Dresden, Germany*
[3] *Institut fur Materialphysik, Universität Göttingen, D-37073 Tammannstr. 1, Göttingen, Germany*
[4] *Institute of Materials Science, Darmstadt University of Technology, D-64287 Petersenstr.23, Darmstadt, Germany*

Abstract

Nanocrystalline thin Nb films loaded with hydrogen were studied in the present work. Thin Nb films were prepared on (100) Si substrates at room temperature by cathode beam sputtering. Microstructure observations by transmission electron microscopy (TEM) revealed that the films exhibit elongated column-like grains. The width of the columns is smaller than 100 nm. Two "generations" of grains can be distinguished in the columns: (i) "first generation" grains attached directly to the Si substrate, and (ii) "second generation" grains which grow on top of the "first generation" grains. X-ray diffraction (XRD) studies revealed that the Nb films are characterized by a strong (110) texture. However, the lateral orientation of grains (i.e. in the plane of the substrate) is random. Defect studies were performed by slow positron implantation spectroscopy (SPIS) with measurement of Doppler broadening (DB) of the annihilation line. The shape of the annihilation line was characterized by the S parameter which represents a fraction of positrons annihilating with low-momentum electrons. It was found that the virgin Nb films (i.e. free of hydrogen) contain a high density of defects. Nanocrystalline grain size leads to a significant volume fraction of grain boundaries containing open volume vacancy-like defects. Thus, most of positrons annihilate from a trapped state in the open volume defects at grain boundaries.

Subsequently, the films were step-by-step electrochemically charged with hydrogen and the evolution of microstructure with increasing hydrogen concentration was monitored. Hydrogen loading leads to a significant lattice expansion which was measured by XRD. Contrary to free standing bulk metals, the lattice expansion is highly anisotropic in thin films. The in-plane expansion is prevented because the films are clamped to an elastically hard substrate. On the other hand, the out-of-plane expansion is substantially larger than in the bulk samples. Moreover, an enhanced hydrogen solubility in the α-phase in the nanocrystalline Nb films is found. Formation of the β-phase (NbH) starts at a hydrogen concentration of $x_H = 0.25$ [H/Nb atomic ratio], i.e. it is ≈ 4 times higher than in bulk Nb. Using SPIS it was found that hydrogen is trapped in vacancy-like defects at grain boundaries. Hydrogen trapping leads to a local increase of the electron density in these defects and is reflected by a pronounced decrease of the S parameter in the hydrogen-loaded samples. Subsequently, when the hydrogen concentration exceeds $x_H = 0.02$ [H/Nb], all available traps at grain boundaries are already filled with hydrogen and the S parameter does not change anymore. Formation of the β-phase particles leads to an introduction of new defects, which is reflected by an increase of the S parameter at $x_H > 0.25$ [H/Nb].

Keywords

Slow positron implantation spectroscopy, Niobium, Hydrogen, Vacancy-like defects, phase diagram

1. Introduction

Metal – hydrogen systems have been extensively studied in the last years. This effort has technological and basic research reasons. On the one hand, the development of optimised hydrogen storage materials is of high importance for a future hydrogen-based technology. On the other hand, a microstructural explanation of the hydrogen-induced deterioration of mechanical properties (embrittlement) of metals is highly desirable. Moreover, it was found that the behaviour of

hydrogen-loaded thin films differs significantly from the behaviour of corresponding bulk materials. Moreover, new hydrogen-related phenomena, e.g. hydrogen-induced optical switching in thin Y films [1], have recently been discovered.

The behavior of hydrogen in a host metal lattice can be influenced significantly by hydrogen interaction with lattice defects. For example, it is well known that hydrogen can be trapped at vacancies [2] and dislocations [3]. Moreover, hydrogen is not only trapped at existing defects but new defects can also be generated by hydrogen loading [4]. Recently it has been found that vacancies surrounded by four hydrogen atoms were created in bulk Nb by electrochemical hydrogen charging [5]. A strong interaction of hydrogen with defects makes defect studies of hydrogen loaded samples highly important for an understanding of the hydrogen behavior in metals. Positron annihilation spectroscopy (PAS) is a well-developed non-destructive technique with a high sensitivity to open-volume defects [6]. Thus, PAS represents an ideal tool for the investigation of hydrogen-defect interactions as well as the characterization of hydrogen-induced defects. Indeed, PAS was employed successfully in various investigations of hydrogen-induced defects in bulk Nb [5]. PAS offers several techniques for defect studies. In the present work we used so-called slow positron implantation spectroscopy (SPIS) for defect studies of thin Nb films loaded with hydrogen. SPIS is the most suitable PAS technique for thin film investigations because it enables defect studies at various depths practically from surface up to several microns. As SPIS is a relatively new technique and is not routinely used in materials science yet, it will be briefly described in section 2. A more detailed treatment of SPIS can be found in [7]. For information about various further applications of SPIS we recommend to see the proceedings [8].

Hydrogen absorption leads to a significant increase of the volume - and thereby also to a lattice expansion - of a sample. The expansion is isotropic in case of free-standing bulk metals. Contrary to bulk material, a thin film usually is clamped to an elastically hard substrate. It prevents the in-plane expansion, while the out-of-plane expansion is remarkably larger compared to that of a free standing bulk metal. As a consequence, hydrogen-induced effects in thin films may differ substantially from those in corresponding bulk materials. Because of this important difference it is highly desirable to compare the hydrogen behavior in thin films with that in bulk samples.

The aim of the present work is the investigation of microstructural changes in hydrogen-loaded thin Nb film. We have chosen Nb because the phase diagram of the Nb-H system is relatively simple and well documented [9]. It is thus advantageous for investigations of the influence of defects on the hydrogen behavior. A bulk Nb-H system represents at room temperature a single phase solid solution (so called α-phase) up to a hydrogen concentration x_H = 0.06 [atomic ratio Nb/H]. In the α-phase, hydrogen occupies the tetrahedral interstitial positions in the bcc Nb lattice. At higher hydrogen concentrations the system becomes a mechanical mixture of two phases: the α-phase and the hydrogen-rich β-phase (NbH) which is an orthorhombic distortion of the bcc Nb lattice.

In the present work, the thin Nb films were step-by-step electrochemically loaded with hydrogen in the range x_H = (0 – 1) and the corresponding development of the microstructure was investigated. Defect studies of thin films were performed by SPIS with measurement of DB of the annihilation line. Hydrogen-induced lattice expansion was detected by XRD. These techniques were combined with a direct observation of the microstructure by TEM.

2. SPIS (Slow Positron Implantation Spectroscopy)

Conventional sources of positrons for PAS are artificial radioisotopes emitting β^+ radiation. By far the most frequently used among them is ^{22}Na. Energy spectra of positrons emitted by such radioisotopes are continuos ranging from zero up to the end-point energy which is typically of the order of 0.1-1 MeV. The energy spectrum of positrons emitted by ^{22}Na is shown in Fig. 1. A positron implantation profile in solids can be described by an exponential function [6]

$$P(z) = a e^{-az}, \quad a\left[\mathrm{cm}^{-1}\right] = 16\frac{d\left[\mathrm{g\,cm}^{-3}\right]}{E_{\max}^{1.4}\left[\mathrm{MeV}\right]}, \qquad (1)$$

where $E_{\max}$ is the end-point energy of emitted positrons (0.545 MeV for ^{22}Na) and d denotes the density of the solid. The mean positron penetration depth a^{-1} can be easily calculated from Eq. (1) - in metals it is typically 10 – 100 μm, and for Nb 31.8 μm is estimated. Thus, positrons emitted by the β^+ emitters probe volume properties of solids and are very suitable for investigations of bulk samples. PAS studies using energetic positrons from radioactive sources are sometimes called ‚conventional PAS‘. A brief overview of conventional PAS and its applications to condensed matter studies and materials science can be found in [10].

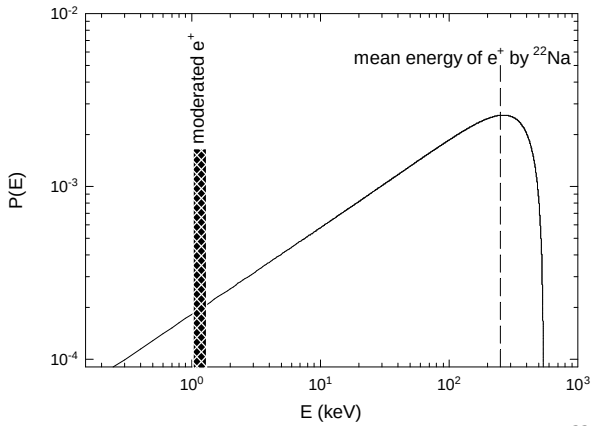

Fig. 1 The energy spectrum of positrons emitted by ^{22}Na is plotted by a solid line, and the hatched area indicates energies of moderated positrons.

Conventional PAS cannot be used for investigations of thin films or surfaces. For such investigations it is necessary to decrease the kinetic energy of positrons. SPIS uses low energy (slow) positrons being thermalized in a moderator. Thereby energetic positrons emitted by the β^+ radioactive source are firstly implanted in vacuum into a moderator. A thin tungsten foil is often used as a moderator because it exhibits a negative positron work function. However, other suitable materials, e.g. Ni or solid Ne, are used as well. Most positrons leave the moderator in a non-thermalized state with slightly lowered but still high energy. Some positrons annihilate in the moderator. A small fraction of positrons (typically 10^{-4}) are thermalized in the moderator (i.e. their energy is lowered down to $\approx kT$) and escape from the moderator (into vacuum) due to the negative work function. Such moderated positrons are practically monoenergetic with an energy of a few eV only. SPIS technique uses a beam of moderated positrons. The moderated positrons are selected from the non-thermalized ones by a E×B filter, or simply by bending of the beam tube which can be followed by the slow positrons only whereas the fast ones hit the tube wall and annihilate there. Subsequently, the moderated positrons are guided by a magnetic field into an accelerator where they are accelerated in an electric field to the desired energy. The positron energy can be varied usually in the range 0.01 - 40 keV. The accelerated positrons are then guided into the sample. Hence, contrary to conventional PAS, SPIS uses a beam of *monoenergetic* positrons with variable energy. A schematic sketch of a SPIS beam is shown in Fig. 2.

The implantation depth of monoenergetic positrons with energy E can be expressed by a Makhovian function [11].

$$P(z) = \frac{m z^{m-1}}{z_0^m} \exp\left[-(z/z_0)^m\right], \qquad (2)$$

where m ≈ 1.9 is a shape parameter and

$$z_0 = \frac{\bar{z}}{\Gamma\left[(1/m)+1\right]}. \qquad (3)$$

where $\bar{z}$ is the mean stopping depth. The dependence of $\bar{z}$ on energy is described by a power law

$$\bar{z} = AE^n, \qquad (4)$$

The constant A was found empirically to be $A \approx 400/r$ Å/keV^n, where r denotes the sample density in g/cm^3, $\bar{z}$ is given in Å, and E is given in keV [12]. The power n ≈ 1.6 holds for most materials [13].

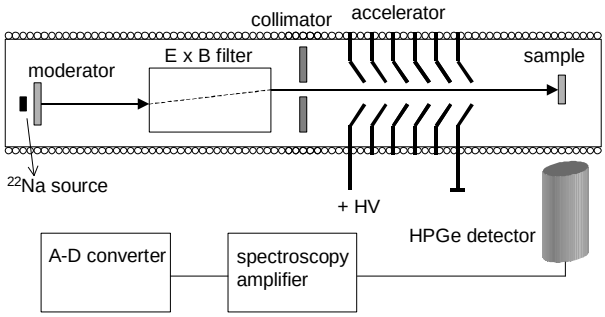

Fig. 2 A schematic sketch of a variable energy slow positron beam used in SPIS.

The implantation profiles of positrons with various energies in Nb are shown in Fig. 3 as an example. Clearly, positrons with higher energy penetrate on average deeper into the sample. Thus, by variation of the positron energy one can investigate a depth profile, i.e. microstructural changes as a function of depth from surface of the studied sample.

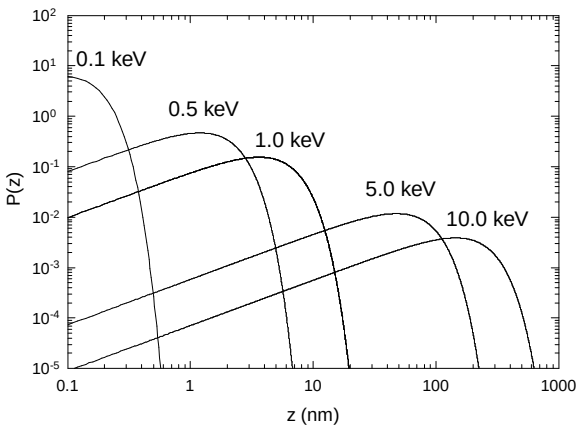

Fig. 3 An example of the implantation profiles of positrons with various energies in Nb.

The electromagnetic interaction between electrons and positrons leads to annihilation of $e^+ - e^-$ pairs in which the total energy of the annihilating pair is transferred to annihilation gamma rays. The

principal channel of this reaction is a two-photon annihilation

$$e^+ + e^- = g_1 + g_2. \quad (5)$$

The DB of the annihilation gamma rays is usually measured in SPIS experiments. As shown in Fig. 4, an electron-positron annihilating pair exhibits non-zero momentum in the laboratory frame. It leads to a Doppler shift *DE* of energies of the two annihilation photons with respect to the rest energy of electron, $E_0 = m_0 c$. The momentum of a thermalized positron is negligible compared to the momentum of an electron. Thus, the Doppler shift *DE* is directly proportional to the electron momentum component p_L in the direction of measurement (see Fig. 4)

$$\Delta E = \pm \frac{1}{2} c p_L, \quad (6)$$

where *c* is the velocity of light.

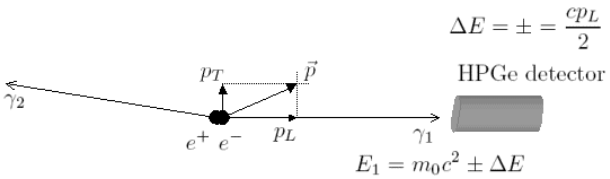

Fig. 4 Kinematics diagram of the two-photon annihilation of e^+ – e^- pair in the laboratory frame. Electron momentum is denoted $\vec{p}$, subscripts L and T denote longitudinal and transversal components, respectively. The longitudinal direction was chosen so that it equals to the direction of measurement, i.e. the direction of emission of the photon g_1, which is detected in detector.

The Doppler shift *DE* leads to a broadening of the annihilation line (DB), which is measured by a high-purity Germanium (HPGe) detector, see Fig. 4. An energy resolution of ≈1.2 keV is normally achieved at 511 keV with a HPGe detector. The shape of the annihilation line is characterized by so-called lineshape parameters S and W, see Fig. 5 for definition. The S parameter is defined as ratio of the central peak area (small *DE*) to the net peak area, while the W parameter expresses the relative contributions of the peak tails (large *DE*) with respect to the total peak area. The S parameter is higher if the relative contribution of lower momentum electrons to positron annihilation is enhanced. On the other hand, the W parameter becomes larger if the contribution of core electrons with higher momentum tends to increase.

A thermalized positron moves through a defect-free crystal lattice in a delocalized state as a quantum-mechanical wave with a wavelength of ≈50 Å. Due to the Coulomb repulsion by positive-ion cores, a positron in a condensed medium preferably resides in the inter-atomic space. The potential sensed by a positron is lowered at open volume defects (vacancies, vacancy clusters, dislocations etc.) due to a reduction in the Coulomb repulsion. As a result, a localized positron state at the defect can have a lower energy than the state of delocalized (free) positron. The transition from the delocalized state to the localized state is called 'positron trapping'. The overlap of the wave function of a positron trapped at an open-volume defect with the core electrons wave functions is reduced compared to the case of a free positron. As a consequence, the annihilation of trapped positrons with core electrons is decreased which leads to an increase of the S parameter.

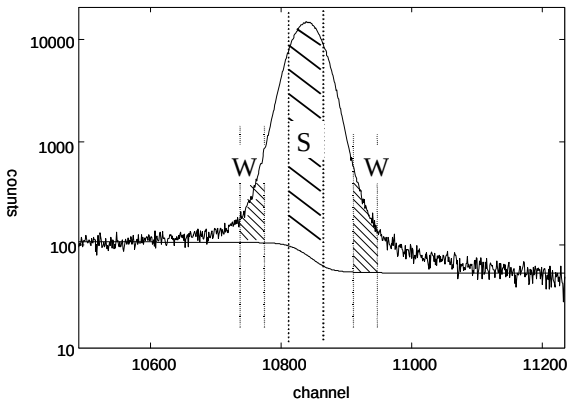

Fig. 5 A schematic depiction of the regions used for the determination of S and W parameters.

3. Experimental Details

Thin Nb films were prepared in an UHV chamber using cathode beam sputtering at room temperature on polished (100) Si substrates. The thickness of the films was determined by profilometry and by TEM as 1,100 (50) nm and 1,120 (20) nm, respectively. The surface of all samples was covered with a 20 nm thick Pd cap in order to prevent oxidation and to facilitate hydrogen absorption [3].

The samples were step-by-step loaded with hydrogen by electrochemical charging, see [3] for details. The charging was done in a galvanic cell by constant current pulses (charge density amounts to 3×10^{-3} mA mm^{-2}) using a Pt counter electrode, while the loaded sample was used as a working electrode. A mixture of H_3PO_4 (85 %) and glycerin (85 %) in the ratio 1:1 served as electrolyte. In order to prevent hydrogen losses, oxygen was removed from the electrolyte by slow rate bubbling with Ar for 24 h prior to the electrochemical charging. The hydrogen concentration in the sample was calculated from Faraday's Law. The voltage between the charged sample and a reference Ag/AgCl electrode was measured. This voltage (so-called EMF) is related to the chemical potential of hydrogen (see [3] for details) and may be used for an independent determination of phase boundaries in the studied films. The EMF measurements were carried out with an impedance converter of high

input resistance and a digital voltmeter connected to a computer.

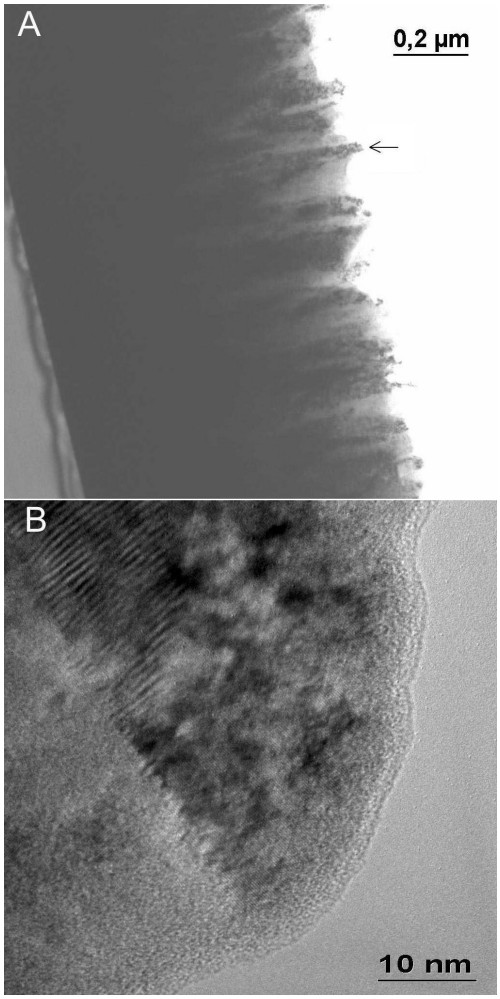

Fig. 6 a) a bright field TEM image of the virgin film, b) a high-resolution image of the region indicated in the upper panel by an arrow.

The SPIS studies of defects in thin films were performed at the magnetically guided positron beam "SPONSOR" [14] with positron energy adjustable from 0.03 to 36 keV. Energy spectra of annihilation gamma rays were measured by a HPGe detector with an energy resolution of (1.09 ± 0.01) keV at 511 keV.

Texture measurements we performed on a four-axis Philips X'pert MPD diffractometer using Co-K_α radiation. XRD measurements of the hydrogen-induced lattice expansion were performed at Hasylab (DESY) using synchrotron radiation with a wavelength of λ = 1.12 Å. The lattice expansion was measured in the out-of-plane direction (i.e. in the direction perpendicular to the film surface which corresponds to $\Psi = 0^o$), and in the direction tilted by $\Psi = 60^o$ with respect to the normal to the surface. In such a way, information about the anisotropy of the film expansion was obtained. Diffraction profiles were fitted by the Pearson VII function.

TEM studies were performed with a Philips CM300 Super TWIN microscope operating at 300 kV. Thin foils for cross sectional TEM were produced by conventional preparation using a Gatan precision ion polishing system (PIPS).

4. Results and Discussion

A bright-field TEM image (cross-section) of the virgin film (i.e. without hydrogen) is shown in Fig. 6a. The sample exhibits "column-like" elongated grains. The widths of the columns do not exceed 100 nm and are found typically to be ~50 nm. A high resolution image of a column is shown in Fig. 6b. The columns are divided horizontally into two "generations" of grains with a height being approximately half the film thickness. The "first generation" grains are attached to the Si substrate, while the "second generation" grains grow on top of the "first generation", i.e. they are situated close to the film surface.

Texture measurements showed that the film exhibits a strong 110 texture, i.e. the grains are oriented predominantly with {110} planes parallel to the surface. However, the lateral orientation of grains (in the plane of the substrate) is random. The diffraction profile shape of the (110) Nb reflection measured on the virgin film is plotted in Figs. 7a,b for the out-of-plane direction ($\Psi = 0^o$) and the direction tilted $\Psi = 60^o$ with respect to the normal to surface. The profiles shown in Figs. 7a,b are a superposition of Nb (110) reflection from the Nb layer and a weak Pd (111) reflection coming from the Pd cap. Moreover, from Fig. 7a is seen that the reflection for $\Psi = 0^o$ is asymmetric and it must be fitted by three different contributions: a weak and broad reflection from the Pd cap, plus two different contribution from the Nb layer corresponding to the inter-planar distance 2.391(2) Å and 2.362(2) Å, respectively. Taking into account the results of TEM observations discussed above, it indicates that the distance d_{110} between the {110} planes in the "first generation" grains (close to the Si substrate) and in the "second generation" grains (close to the film surface) differs. It should be mentioned that the distance between the {110} planes in bulk Nb is d_{110} = 2.3338 Å [15] (the dashed line in Figs. 7a,b). Similarly, the distance between the {111} planes in bulk Pd is indicated in Figs. 7a,b by another dashed line. It is clear that the out-of-plane distance d_{110} in the Nb layer (both generations of grains) as well as d_{111} in the Pd over-layer are significantly larger than in the corresponding bulk materials. It indicates the existence of compressive stresses in the in-plane direction caused by a mismatch of inter-atomic spacing in the Nb film and the Si substrate. The compressive stress leads to an anisotropy of d_{110}, so

that d_{110} is larger than that for bulk Nb in the out-of-plane direction, while in the in-plane direction it is smaller. The "first generation" grains are attached directly to the Si substrate which leads to the highest mismatch of inter-atomic spacing. On the other hand, the "second generation" grains grow on top of the "first generation" and the mismatch is, therefore, smaller. Thus, we can attribute d_{110} = 2.391(2) Å to the "first generation" grains where the compressive stresses are higher, while d_{110} = 2.362(2) Å (closer to the Nb bulk value) can be attributed to the "second generation" grains which are more relaxed. The distance between the {110} planes in the direction tilted $\Psi = 60^o$ with respect to normal to the surface is remarkably smaller compared to the out-of-plane direction and practically coincides with d_{110} for bulk Nb, see Fig. 7b. The d_{110} distances for the two generations of sub-columns are in this case too close to each other in order to become separated in the XRD spectrum.

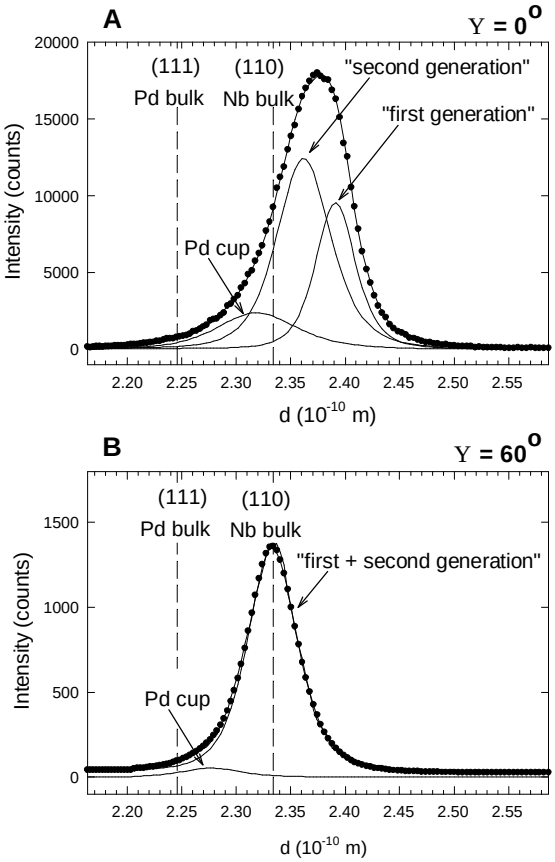

Fig. 7 XRD diffraction profile for the virgin film a) direction out-of-plane, $\Psi = 0^o$, b) direction tilted $\Psi = 60^o$ with respect to normal to the surface. Fits of the experimental points are plotted by thick solid lines, while the thin solid lines show the individual reflections which contribute to the profile. The distance between the {110} and {111} planes in bulk Nb and Pd, respectively, is indicated by the dashed vertical lines.

The inter-planar distances d_{110} in the out-of-plane direction for both generations of grains and d_{110} for the direction $\Psi = 60^o$ are plotted in Fig 8 as a function of x_H. One can see in the Figure that d_{110} exhibits an increase with x_H which is approximately linear in the α-phase field. However, there is a change of slope of the film expansion in the out-of-plane direction at x_H = 0.06, see Fig. 8. Formation of the β-phase starts above x_H = 0.25. It is demonstrated clearly in the direction $\Psi = 60^o$ by the appearance of a new diffraction profile which corresponds to the (200) reflection from the β-phase. Thus, in the case of β-phase the inter-planar distance shown in Fig. 8 corresponds to the distance between the {200} planes. In the out-of plane direction it was not possible to separate the contribution which comes from the β-phase because of a more complicated structure of the diffraction profile. Nevertheless, the start of the β-phase formation is indicated by an increase of the width of this reflection. In the range from x_H = (0.25 0.60) the film represents a mechanical mixture of the α–phase and the hydrogen-rich β-phase. The volume fraction of the β-phase increases with x_H. Eventually, at higher concentrations $x_H > 0.60$, the film is completely transformed into the β-phase. The maximum hydrogen solubility in bulk Nb at room temperature is 0.06. Hence the film exhibits a four times higher solubility of hydrogen in the α-phase compared to bulk Nb. The extended hydrogen solubility could be due to the nanocrystalline grains. Their presence leads to a significant volume fraction of grain boundaries which can accumulate more hydrogen atoms. An enhanced hydrogen solubility in thin Nb films has already been reported in [16].

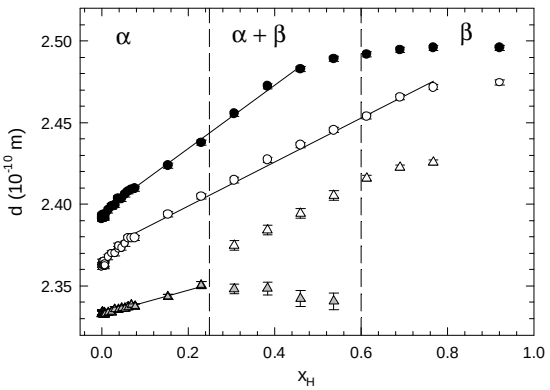

Fig. 8 Dependence of the inter-planar distance d on hydrogen concentration x_H in the film. Full circles – d_{110} "first generation" grains, $\Psi = 0^o$; open circles – d_{110} "second generation" grains, $\Psi = 0^o$; gray triangles d_{110}, $\Psi = 60^o$; open triangles d_{200}, β-phase, $\Psi = 60^o$.

The dependence of the EMF on x_H is plotted in Fig. 9. EMF exhibits a dramatic decrease in the interval x_H = (0.25 - 0.60) due to formation of the β-phase. This finding is in good agreement with the phase

boundaries determined by XRD. In addition, there is a change of slope of the EMF dependence at x_H = 0.007. This effect will be discussed later in connection with SPIS results.

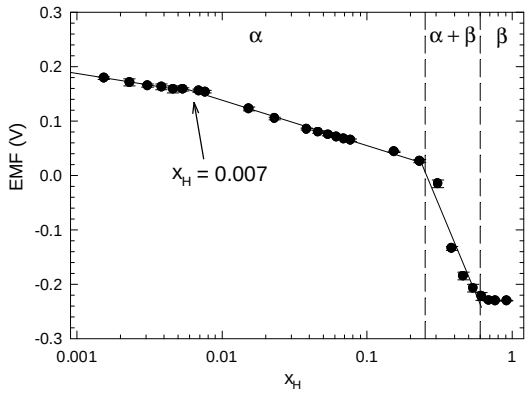

Fig. 9 Dependence of EMF on hydrogen concentration. Positions of phase boundaries are indicated by vertical dashed lines.

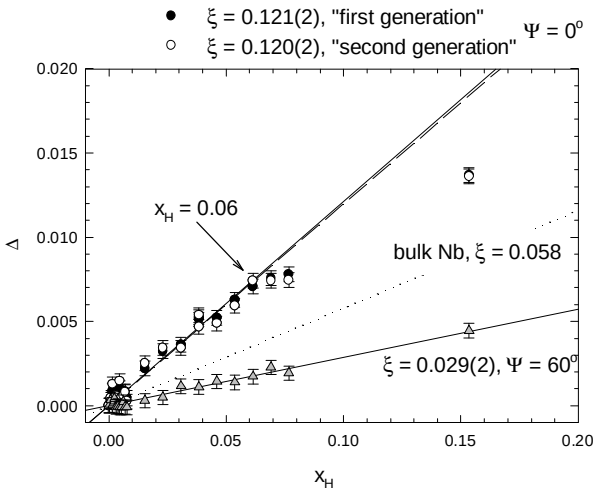

Fig. 10 Hydrogen-induced relative lattice expansion Δ as a function of hydrogen concentration x_H. Dependence of the inter-planar distance d on hydrogen concentration x_H in the film. Full circles – "first generation" grains, Ψ = 0°; open circles – "second generation" grains, Ψ = 0°; gray triangles - Ψ = 60°. The relative lattice expansion for bulk Nb is shown by dotted line.

The relative lattice expansion

$$\Delta(x_H) = [d(x_H) - d_0]/d_0, \qquad (7)$$

where d_0 and $d(x_H)$ represent the inter-planar distance in the virgin sample and the one loaded to a hydrogen concentration x_H, respectively, is plotted in Fig. 10 as a function of x_H in the α-phase field (i.e. for $x_H < 0.25$). The relative lattice expansion in bulk Nb is isotropic and in the α-phase region it is directly proportional to the hydrogen concentration, i.e.

$$\Delta(x_H) = x\, x_H. \qquad (8)$$

The materials constant $x = 0.058$ can be found in the literature for bulk Nb [9]. On the other hand, the in-plane expansion of the thin film is prevented by clamping it to the elastically hard substrate. XRD studies of the hydrogen loaded thin films turned out that the film expansion in the in-plane direction is very small (if any) while the out-of-plane expansion is substantially larger than in a free standing bulk sample [17]. It can be seen from Fig. 10 that $\Delta(x_H)$ in the out-of-plane direction is the same for both generations of grains, and it is significantly larger than in bulk Nb (shown by a dotted line). On the other hand, $\Delta(x_H)$ in the direction Ψ = 60° is smaller than in bulk Nb. Moreover, there is a change of slope of the out-of-plane expansion at x_H = 0.06. Such an effect does not occur in bulk Nb and indicates some change of mechanism of the film expansion.

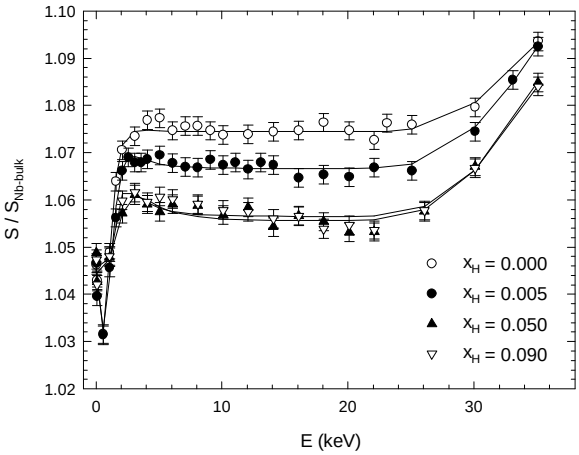

Fig. 11 Selected S(E) curves for the virgin film and the film loaded to various concentrations of hydrogen.

SPIS measurement of a reference (well annealed, defect free) bulk Nb sample revealed the bulk value of the S parameter to be $S_{Nb\text{-}bulk}$ = 0.5095(3), and a positron diffusion length L_+ = 310 (10) nm.

The dependence of the S parameter on positron energy E for the virgin film and for selected hydrogen concentrations is plotted in Fig. 11. Values of S parameter were normalized to the defect-free value $S_{Nb\text{-}bulk}$. A drop of S at low energies is due to positron annihilations inside the Pd cap. It was confirmed by the measurement of a reference 1000 nm thick Pd film sputtered under the same conditions as the Nb films. An increasing fraction of positrons annihilating inside the Nb layer is reflected by an increase of S parameter with increasing energy E, starting from E = 1 keV. In the interval E = (4 - 22) keV virtually all positrons annihilate inside the Nb layer and the S parameter remains approximately constant. Eventually, at energies E > 22 keV some positrons penetrate into the Si substrate which results in a further increase

of the S parameter. The solid lines in Fig. 11 represent a fit performed using the VEPFIT software package [18], with assuming three layers (i.e. Pd cap, the Nb layer, and the Si substrate). From Fig. 11 it is clear that the virgin film exhibits $S/S_{Nb\text{-}bulk} \approx 1.075$ in the Nb layer. Thus, the S parameter in the Nb layer, S_{Nb}, in the virgin sample is substantially higher than the bulk value for defect-free bulk Nb. The positron diffusion length $L_+ = 20$ nm is estimated for the Nb layer from fitting of the S(E) curve for the virgin film. Thus, it can be concluded that the virgin film exhibits a high density of defects. From comparison with TEM results it can be seen that the width of the columns determined by TEM is about three times smaller than L_+ in defect-free bulk Nb. Thus, there is a high probability for any free positron to diffuse to a grain boundary (GB), i.e. to the interface between the columns, and to become trapped at an open volume defect there. Therefore, we assume that most of the positrons in the virgin film are trapped at open volume defects at the interfaces between the columns. Structure of the interfaces is not known but they can hardly be considered as conventional grain boundaries known from bulk polycrystalline materials. In particular, one can expect enhanced concentration of open-volume defects at the interfaces. It should be mentioned that a similar value of $S/S_{Nb\text{-}bulk}$ was measured in Nb layer in epitaxial film sputtered at 800°C on a sapphire substrate. From high-resolution TEM studies [19] it is known that the epitaxial Nb film exhibits a dense network of misfit dislocations which trap positrons. Similar values of S parameter in both kinds of films indicates that positrons are trapped at vacancy-like defects at the interfaces between the columns. Larger vacancy agglomerates can be ruled out because they are not stable in the epitaxial films sputtered at high temperatures.

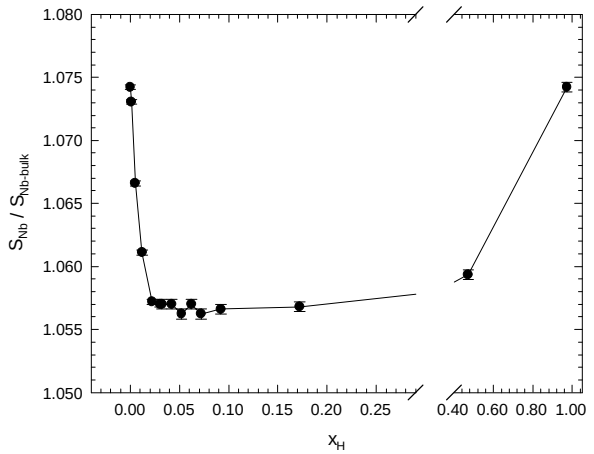

Fig. 12 Dependence of the S parameter for a Nb layer, S_{Nb}, obtained from fitting of the S(E) curves, on hydrogen concentration x_H .

It can be seen in Fig. 11 that S_{Nb} decreases for hydrogen loaded films. This indicates that similarly to positrons also hydrogen is trapped at the open-volume defects at GB's. It was proved both by theoretical calculations and experimentally that a vacancy-like defect with one or more hydrogen atoms attached is still able to trap positrons [5]. However, the presence of hydrogen bound to such defects leads to an increase of the local electron density at the defect and, thereby, to a decrease of the lifetime of trapped positrons. In addition, the positron binding energy to the defect becomes lower. As a consequence, the overlap of the positron wave function with high momentum core electrons increases and leads to a decrease of the S parameter. The dependence of S_{Nb} obtained from fittings of the S(E) curves on x_H is plotted in Fig. 12. Starting from a virgin film, hydrogen firstly fills gradually the open-volume defects at GB's. This is seen as a rapid decrease of S_{Nb}. Above $x_H = 0.02$, all the available open-volume traps at GB's are already filled. The local concentration of hydrogen in the vicinity of the defects reaches a steady state value, and S_{Nb} does not change anymore. A high mobility of hydrogen in Nb at room temperature [5] ensures that if there is any open volume trap available, then the hydrogen atom likely finds it. Hence, at low concentrations of hydrogen practically all hydrogen atoms may be trapped at the defects at GB's. The change of slope of the EMF dependence at $x_H = 0.007$ (Fig. 9) may be then interpreted as the concentration above which hydrogen is not situated exclusively at GB's but starts to occupy also the "regular" tetrahedral interstitial positions inside the grains. The formation of the β-phase takes place at $x_H > 0.25$. It is known that dislocation loops may be emitted by growing particles of hydrides [20]. In addition, positrons can be trapped at misfit defects at the interface between a β-phase precipitate and the matrix. Indeed, as one can see in Fig. 12, S_{Nb} exhibits an increase at $x_H > 0.25$ due to formation the β-phase particles. Thus, we can conclude that the formation of β-phase particles leads to the formation of new open-volume defects.

5. Conclusions

In the present work, defect studies of hydrogen loaded nanocrystalline thin Nb film of a thickness ≈ 1.1 μm were performed. The film exhibits a high density of defects already in the virgin state. Most of the positrons annihilate from a trapped state at open-volume defects at grain boundaries. It was found that the hydrogen solubility in the α-phase in the film is four times higher compared to bulk Nb. The

hydrogen-induced lattice expansion of the film exhibits a strong anisotropy: the out-of-plane expansion is significantly larger than in bulk Nb, while the expansion in the direction tilted by $\Psi = 60^{o}$ with respect to normal to the film surface is remarkably smaller. SPIS measurements revealed that hydrogen is trapped at open-volume defects at grain boundaries which is reflected by a decrease of the S parameter. No formation of new defects was found in the α-phase region. On the other hand, the formation of β-phase particles leads to an increase of the defect density.

Acknowledgements

This work was supported by The Czech Science Foundation (contract No.202/05/0074) and The Ministry of Education, Youth and Sports of Czech Republic (project MS 0021620834).

References

1. J.N. Huiberts, R. Griessen, J.H. Rector, R.J. Wijngaarden, J.P. Dekker, D.G. de Groot, N.J. Koeman, *Nature* (London) **380**, 231 (1996).
2. B. Lengeler, S. Mantl, W. Triftshäuser, *J. Phys. F* **8** (1978) 1691.
3. R. Kircheim, *Prog. Mat. Sci.* **32** (1988) 261.
4. Y. Fukai, N. Ökuma, *Phys. Rev. Lett.* **73**, 1640 (1994).
5. J. Čížek, I. Procházka, F. Bečvář, R. Kužel, M. Cieslar, G. Brauer, W. Anwand, R. Kirchheim, A. Pundt, *Phys. Rev. B* **69** (2004) 224106.
6. P. Hautojärvi, C. Corbel, in: *Positron Spectroscopy of Solids*, Eds. A. Dupasquier and A.P. Mills, Jr., IOS Press, Amsterdam 1995, p. 491.
7. P.J. Schultz, K.G. Lynn, *Rev. Mod. Phys.* **60**, 701 (1988).
8. *Applied Surface Science* **194** (2002): *Proceedings of the 9th International Workshop on Slow-Positron Beam Techniques for Solids and Surfaces*, Eds. G. Brauer, W. Anwand, Elsevier, Amsterdam 2002.
9. T. Schober, H. Wenzl, in: *Hydrogen in Metals II*, Topics in Applied Physics Vol. 29, Eds. G. Alefeld and J. Völkl, Springer, Berlin, 1978, p. 32.
10. I. Procházka, *Materials Structure* **8**, 55 (2001).
11. A.F. Makhov, *Fiz. Tverd. Tela (Peterburg)* **2**, 2161 (1960).
12. A.P. Mills, R. Wilson, *Phys. Rev. A* **26**, 490 (1982).
13. K.G. Lynn, H. Lutz, *Phys. Rev. B* **22**, 4143 (1980).
14. W. Anwand, H.-R. Kissener, G. Brauer, *Acta Phys. Polonica A* **88**, 7 (1995).
15. ICDD (International Centrum for Diffraction Data) Powder diffraction pattern database PDF-2.
16. S. Moehlecke, C.F. Majkrzak, M. Strongin, *Phys. Rev. B* **31**, 6804 (1985).
17. H. Peisl, in: *Hydrogen in Metals I*, Topics in Applied Physics Vol. 28, Eds. G. Alefeld and J. Völkl, Springer, Berlin 1978, p. 53.
18. A. van Veen, H. Schut, M. Clement, J. de Nijs, A. Kruseman, M. Ijpma, *Appl. Surf. Sci.* **85**, 216 (1995).
19. G. Gutekunst, J. Mayer, M. Rühle, *Phil. Mag. A* **75**,
20. 1329 (1997).
21. C. Borchers, U. Laudahn, A. Pundt, S. Fähler, H.U. Krebs, R. Kirchheim, *Philos. Mag. A* **80**, 543 (2000).